Original Article

Evaluation of a fast-volumetric four-dimensional magnetic resonance imaging technique for abdominal radiotherapy tumor motion management

Peilin Wang[1#], Weiwei Liu[2#], Haonan Xiao[1], Chenyang Liu[1], Wen Li[1], Ge Ren[1], Yibao Zhang[2], Hao Wu[2], Weihu Wang[2], Jing Cai[1], Tian Li[1]

[1]Department of Health Technology and Informatics, The Hong Kong Polytechnic University, Hong Kong, China; [2]Key Laboratory of Carcinogenesis and Translational Research (Ministry of Education/Beijing), Department of Radiation Oncology, Beijing Cancer Hospital & Institute, Peking University Cancer Hospital & Institute, Beijing, China

Contributions: (I) Conception and design: W Liu, T Li; (II) Administrative support: H Wu, W Wang, J Cai; (III) Provision of study materials or patients: H Wu, W Wang; (IV) Collection and assembly of data: H Wu, W Wang; (V) Data analysis and interpretation: P Wang, W Liu, H Xiao, C Liu, T Li; (VI) Manuscript writing: All authors; (VII) Final approval of manuscript: All authors.

[#]These authors contributed equally to this work.

Correspondence to: Jing Cai, PhD; Tian Li, PhD. Department of Health Technology and Informatics, The Hong Kong Polytechnic University, 11 Yuk Choi Rd., Hung Hom, Hong Kong, China. Email: jing.cai@polyu.edu.hk; tianli@polyu.edu.hk.

Background: Motion management plays an important role in abdominal cancer radiotherapy. In this study, we investigated the motion measurement accuracy and tumor contrast in liver tumor using a fast volumetric four-dimensional magnetic resonance imaging (4D-MRI) technique using commercial sequence.

Methods: Four volunteers and 34 patients with liver tumors were included in this study with institutional review board (IRB) approval, and all patients underwent routine MRI scans with additional 4D-MRI scan on a 3.0 Tesla MRI scanner. A fast-volumetric sequence [time-resolved imaging with stochastic trajectories-volumetric interpolated breath-hold examination (TWIST-VIBE)] was used to acquire 4D-MRI images. The temporal resolution of 4D-MRI was ~0.69 s per measurement. The 4D-MRI sequence was performed before and immediately after the injection of gadolinium contrast agent, termed as non-contrast 4D-MRI (in patient study) and contrast-enhanced 4D-MRI (4D-MRI$_{CE}$) respectively. The tumor average motion amplitude (AMA) and maximum motion amplitude (MMA) in the superior-inferior (SI), anterior-posterior (AP), and medium-lateral (ML) directions were measured in two sets of 4D-MRI and three sets of two-dimensional (2D) Cine magnetic resonance (MR) images. The tumor signal-to-noise ratio (SNR) and tumor-to-liver contrast-to-noise ratio (CNR) were also evaluated.

Results: High temporal resolution (~0.69 s per measurement) and isotropic spatial resolution (~2.7 mm^3 voxel size) were achieved with the fast volumetric 4D-MRI technique. Phantom experiments validated the motion measurement accuracy, showing that the average and MMAs in the SI, AP, and ML directions matched the programmed motions with errors below 3 mm. In patient studies, tumor motion amplitudes and trajectories measured by 4D-MRI$_{CE}$ and non-contrast 4D-MRI (4D-MRI$_{NC}$) were comparable to conventional 2D Cine MRI in all three directions, with no statistically significant differences. Specifically, for AMA, the P values were 0.096, 0.019, and 0.009 for 4D-MRI$_{CE}$ in the SI, AP, and ML directions, respectively, and 0.049, 0.008, and 0.016 for 4D-MRI$_{NC}$, respectively. For MMA, the corresponding P values were 0.054, 0.022, and 0.086 for 4D-MRI$_{CE}$, and 0.041, 0.007, and 0.016 for 4D-MRI$_{NC}$. Tumor SNR and tumor-to-liver CNR obtained with 4D-MRI$_{CE}$ and 4D-MRI$_{NC}$ were also comparable to those from standard diagnostic sequences (T1W, T2W) and Cine MRI, with P values <0.05, ensuring sufficient image quality for radiotherapy planning. Although minor motion artifacts were occasionally observed, the overall image

quality and motion fidelity support the clinical feasibility of the method. Taken together, these results demonstrate that the TWIST-VIBE 4D-MRI technique provides accurate, high-quality volumetric motion assessment efficiently, without requiring specialized hardware or prolonged scanning times.

Conclusions: Our preliminary results demonstrated that the commercially available TWIST-VIBE 4D-MRI sequence provides precise volumetric tumor motion tracking suitable for clinical abdominal radiotherapy. Its rapid acquisition and reliable image quality facilitate seamless workflow integration, potentially enhancing treatment precision and improving patient outcomes. The technique offers a practical alternative to existing imaging modalities by combining speed, spatial coverage, and soft tissue contrast without additional hardware requirements. Further efforts will target artifact minimization, optimization of spatial and temporal resolutions, improved clinical decision-making impact, and broader multi-center validation to ensure robust clinical implementation and generalizability across diverse patient populations.

Keywords: Four-dimensional magnetic resonance imaging (4D-MRI); liver cancer; tumor motion; time-resolved imaging with stochastic trajectories-volumetric interpolated breath-hold examination (TWIST-VIBE); radiotherapy planning

Submitted Feb 28, 2025. Accepted for publication Aug 27, 2025. Published online Sep 13, 2025.
doi: 10.21037/qims-2025-1039
View this article at: https://dx.doi.org/10.21037/qims-2025-1039

Introduction

Abdominal cancers are a leading cause of cancer related morbidity and mortality. According to the report of the World Health Organization, the number of new liver cancer and pancreatic cancer around the world were 906 thousand and 496 thousand in 2020, located on the 6th and 13th among all malignant tumors, respectively (1). While the cancer related death of liver cancer and pancreatic cancer were 830 thousand and 446 thousand in 2020, ranking at 2nd and 7th among all malignant tumors, respectively. In the past ten years, radiation therapy has made great progress as one of the treatment methods for abdominal cancer, especially with the development of stereotactic-body radiotherapy (SBRT) in recent years which greatly improves the local tumor control rate of abdominal cancer (2-7). However, the application of radiotherapy in abdominal cancer is still limited due to the radiation toxicity to normal tissues and the respiratory motion is the main obstacle to further improve the efficacy of radiotherapy for abdominal cancer (7-9).

Therefore, respiratory motion management, which refers to the procedures that sense and account for motion, plays an important role in abdominal cancer radiotherapy (10). If not properly managed, the respiratory motion can compromise the treatment accuracy and cause underdose to the target or overdose to the normal tissues. Recently, four-dimensional imaging has been used for respiratory motion management in radiotherapy, especially the tumor and organ motion measurement. In clinical practice, four-dimensional computed tomography (4D-CT) is the clinical standard technique for motion measurement (11). However, due to the low soft tissues contrast of CT, it is difficult for 4D-CT to clearly show the location of the tumor in the abdomen.

Magnetic resonance imaging (MRI) on the contrast offers excellent soft tissue contrast without ionizing radiation, drawing increasing attention in radiotherapy. While two-dimensional (2D) Cine MRI has been used for tumor motion assessment (12,13), its repeated acquisitions in multiple directions are inefficient. Four-dimensional MRI (4D-MRI) overcomes this by providing simultaneous multidirectional tumor motion information. Compared to conventional 2D Cine MRI and slower 3D acquisitions, fast volumetric 4D-MRI sequences such as time-resolved imaging with stochastic trajectories-volumetric interpolated breath-hold examination (TWIST-VIBE) enable high temporal (~0.69 s/measurement) and isotropic spatial (~2.7 mm^3 voxel size) resolution imaging, allowing comprehensive characterization of respiratory-induced tumor displacement. Over the past decades, several 4D-MRI methods have been proposed for abdominal imaging and demonstrated promising results for volunteers and patients. *Figure 1* demonstrated an example of comparison of tumor contours generated from 4D-CT and 4D-MRI. It can be

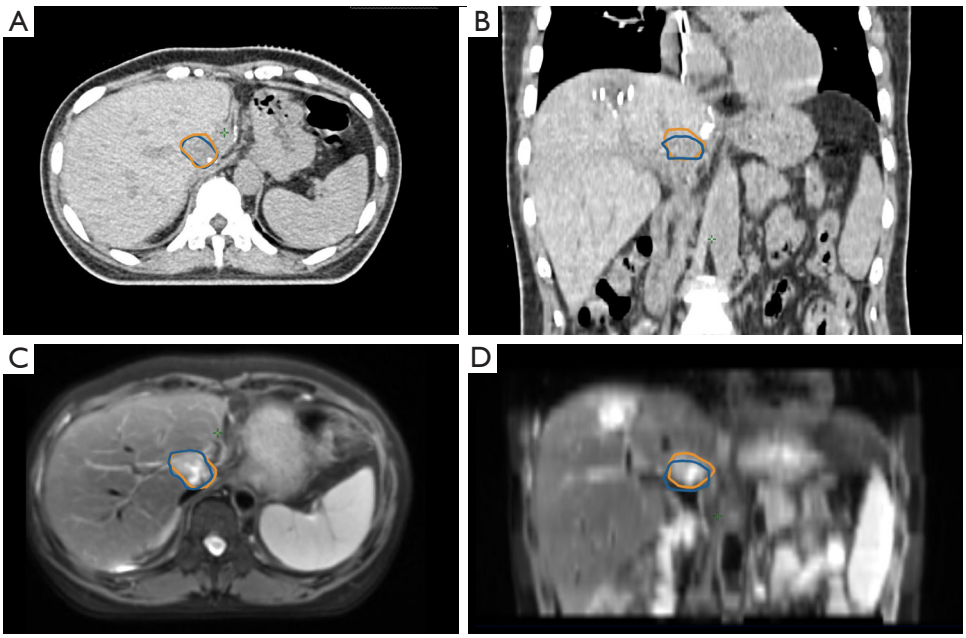

Figure 1 An example of comparison of tumor contours generated from 4D-CT and 4D-MRI. The orange outline is the contour from 4D-MRI and the blue outline is the contour from 4D-CT. (A,B) The CT images in the axial and coronal views; (C,D) the MRI images in the axial and coronal views. 4D, four-dimensional; CT, computed tomography; MRI, magnetic resonance imaging.

seen that the 4D-MRI can provide superior tumor contrast compared to 4D-CT and therefore can potentially improve the accuracy of tumor motion management.

The rich motion information in fast-volumetric 4D-MRI enhances radiotherapy planning accuracy by improving internal target volume (ITV) delineation and motion management strategies. Accurate tumor motion delineation is critical to minimize radiation exposure to healthy tissues, thereby potentially improving treatment efficacy and reducing toxicity. Integrating fast volumetric 4D-MRI into clinical workflows holds promise for more precise and adaptive radiotherapy, a crucial step toward improved patient outcomes.

Specifically, most 4D-MRI techniques can be categorized into two groups: (I) retrospective 4D-MRI; and (II) prospective 4D-MRI. In retrospective 4D-MRI, images are continuously acquired with simultaneous breathing signal recorded and retrospective sorting methods are applied to generate 4D-MRI. For example, Cai *et al.* developed a 4D-MRI technique with 2D fast T_2/T_1-weighted steady-state free precession magnetic resonance (MR) sequence and an image-based surrogate was used for retrospective sorting (14). However, this method requires extra scanning time to acquire enough data for sorting and the image quality may be impaired by breathing irregularity. In prospective 4D-MRI, real-time 3D acquisition or fast 2D acquisition with respiratory triggering system is typically used for image acquisition. For example, Du *et al.* developed a prospective amplitude-triggered 4D-MRI protocol that offers T_2 weighting for better tumor visualization (15). However, the triggering system will prolong the acquisition time especially for irregular breathing patients. For real-time 3D acquisition, Yuan *et al.* proposed a 4D-MRI technique using commercial 3D VIBE sequence with controlled aliasing in parallel imaging. They achieved a spatial resolution of 2.7×2.7×4.0 mm^3 and a time resolution of 0.615 s/measurement (16). However, only nine volunteers were involved in their study and did not investigate this technique in real clinical setting. Therefore, in this study, we aim to investigate a fast-volumetric 4D-MRI technique using commercial sequence for motion management in physical phantom, volunteers, and liver cancer patients. We present this article in accordance with the STARD reporting checklist (available at https://qims.amegroups.

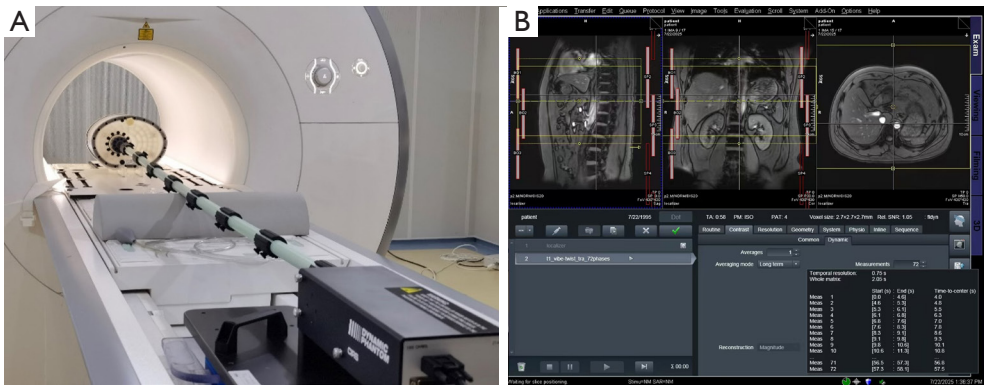

Figure 2 Photographs of the phantom in the MR device and the SCOUT scan of the 4D-MRI. (A) The CIRS (Virginia, USA) MR compatible motion phantom set up for the evaluation of the 4D-MRI motion measurement accuracy. (B) SCOUT scan of 4D-MRI. 4D, four-dimensional; MR, magnetic resonance; MRI, magnetic resonance imaging; SCOUT, synthetic correlated overview utilizing tomography.

com/article/view/10.21037/qims-2025-1039/rc).

Methods

Subjects

A total of four volunteers and 34 patients (age range: 28–78 years, 25 males, 9 females) with liver tumor(s) were included in this study. The study was approved by ethics board of Peking University Cancer Hospital & Institute (No. 2021YJZ05), and informed consent was taken from all the patients. This study was conducted in accordance with the Declaration of Helsinki and its subsequent amendments. The patient cohort comprised individuals with 17 hepatocellular carcinoma (HCC) patients, 13 liver metastases patients, and four post-operative cases. Motion measurements were performed using the visible tumor as a landmark for patients with HCC and liver metastases. For post-operative patients, alternative surrogates such as the gallbladder, liver dome, or post-surgical fluid collections were used for motion assessment. A Computerized Imaging Reference Systems, Inc. (CIRS) (Model 008M, Virginia, USA) MR compatible motion phantom was also used to evaluate the accuracy of motion measurement of the 4D-MRI sequence as shown in *Figure 2*. The phantom is comprised of a plastic shell with a cylindrical thru hole and has a moving rod with a simulated target. The maximum motion amplitude (MMA) is 5.0 cm and the motion accuracy is 0.01 cm. The cycle time is adjusted based on the motion amplitude with a minimum cycle time of one second.

Image acquisition and processing

All the subjects and the phantom have undergone routine MRI scans with additional 4D-MRI scan on a 3.0 Tesla MRI scanner (Skyra, Siemens Healthineers, Erlangen, Germany). The patients were all immobilized using thermoplastic masks and positioned the same as in the radiotherapy process. The 4D-MRI is achieved using TWIST-VIBE sequence with the following scanning parameters: TR =3.44 ms; TE =1.23 ms/2.46 ms; flip-angle =5°; matrix size =160×128; voxel size =2.7×2.7×2.7 mm^3; acquisition time =53 s; number of measurements =72; bandwidth =1,420 Hz/Px. The scanning range covered the whole liver with at least 5.0 cm extension in superior-inferior (SI) direction. Dixon fat suppression was used to suppress the fat signal. The temporal resolution of 4D-MRI was ~0.69 s/measurement, while it takes ~4 s to prepare before the first measurement is collected. The 4D-MRI sequence was performed before and immediately after the injection of gadolinium contrast agent, termed as non-contrast 4D-MRI (4D-MRI_{NC}) and contrast-enhanced 4D-MRI (4D-MRI_{CE}) respectively, without interfering with the clinical scans. All the patients also underwent contrast-enhanced 3D T1-weighted (T1W), 2D gated T2-weighted (T2W), DWI with b=50 and 1,000 s/mm^2, and Cine MRI in three orthogonal directions. The b-value in DWI quantifies the strength of diffusion weighting, determined by gradient amplitude, duration, and timing. Lower b-values (e.g., 50 s/mm^2) provide higher signal-to-noise ratio (SNR) and depict more anatomical detail, whereas higher b-values (e.g., 1,000 s/mm^2) enhance

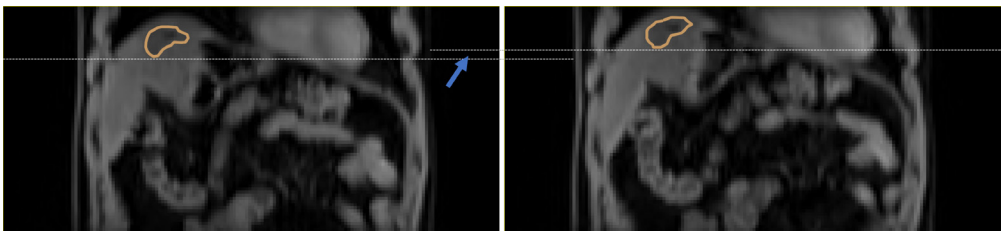

Figure 3 An example of MMA measurement for a patient. The MMA was measured as the distance indicated by the blue arrow. The orange outline represents the tumor contour. MMA, maximum motion amplitude.

sensitivity to restricted water diffusion, which aids in differentiating tissues such as tumors, inflammation, and necrosis. The contrast-enhanced 3D T1W MRI was scanned with stack-of-stars VIBE (STAR-VIBE) sequence after the injection of contrast agent under free-breathing condition with acquisition time around 3 minutes. The scanning parameters for Cine MRI are: TR =249.60 ms; TE =1.22 ms; voxel size =1.3×1.3×8.0 mm^3; acquisition time =13 s; number of measurements =50. Since the patient's breathing curve varies greatly from person to person, a general sinusoidal pattern was used for CIRS motion phantom in SI, anterior-posterior (AP), and medium-lateral (ML) directions with 1.0, 2.0, 3.0, and 4.0 cm amplitudes. The phantom was scanned using the 3D T1W and 4D-MRI sequence with the same parameters as used in patient study.

Data analysis

All the acquired images were analyzed using an in-house developed Matlab (The MathWorks Inc., Natick, Massachusetts, USA) program. For phantom study, the motion amplitude automatically measured in three directions from 4D-MRI using the in-house developed program was compared with the gold-standard, which is the motion amplitude set in the phantom software. The program can automatically segment the moving target of the phantom using threshold-based method and the centroid will be extracted in each frame for the subsequent measurement. The average motion amplitude (AMA) across different motion cycles and MMA of the phantom with different motion amplitudes were also measured. The measurement in SI direction was conducted in both coronal and sagittal views, while the measurement in AP direction was conducted in both axial and sagittal views. The measurement in ML direction was conducted in both axial and coronal views.

In patient study, tumor-to-liver contrast-to-noise ratio (CNR) and SNR were measured for both 4D-MRI_{CE} and 4D-MRI_{NC} sequences to evaluate image quality. This comparison was performed to assess whether non-contrast 4D-MRI could provide sufficient image quality for accurate tumor delineation and motion assessment, thereby offering a clinically preferable alternative that avoids the risks and invasiveness associated with contrast administration.

Besides, the AMA and MMA in the SI, AP, and ML directions were manually measured by an experienced medical physicist in two sets of 4D-MRI and three sets of 2D Cine MR images for all patients. An example of MMA is shown in *Figure 3*. The AMA was measured over five breathing cycles considering the balance between complicity and time consumption. The tumor SNR and tumor-to-liver CNR were measured in 4D-MRI, 2D Cine, T1W, and T2W images. The SNR was measured as the ratio of the mean pixel value to the standard deviation of the pixel values in a selected region. The CNR was measured as the ratio of the mean pixel value difference between tumor and liver to the standard deviation of the pixel values in liver. In addition, retrospective sorting was also applied to the 4D-MRI images to demonstrate the feasibility for radiotherapy application. The volunteer images were only used for feasibility demonstration of the technique and no measurement was done in this cohort.

Results

Phantom study

Figure 4 shows an example of T1W and one frame of 4D-MRI images of the CIRS motion phantom with 1.0 cm motion. It can be seen from *Figure 4B,4C* that the target in the phantom in T1W MRI is blurred due to the motion while the 4D-MRI can resolve the motion clearly without blurring as the blue arrow shows. The motion amplitude measurement results in three directions are shown in

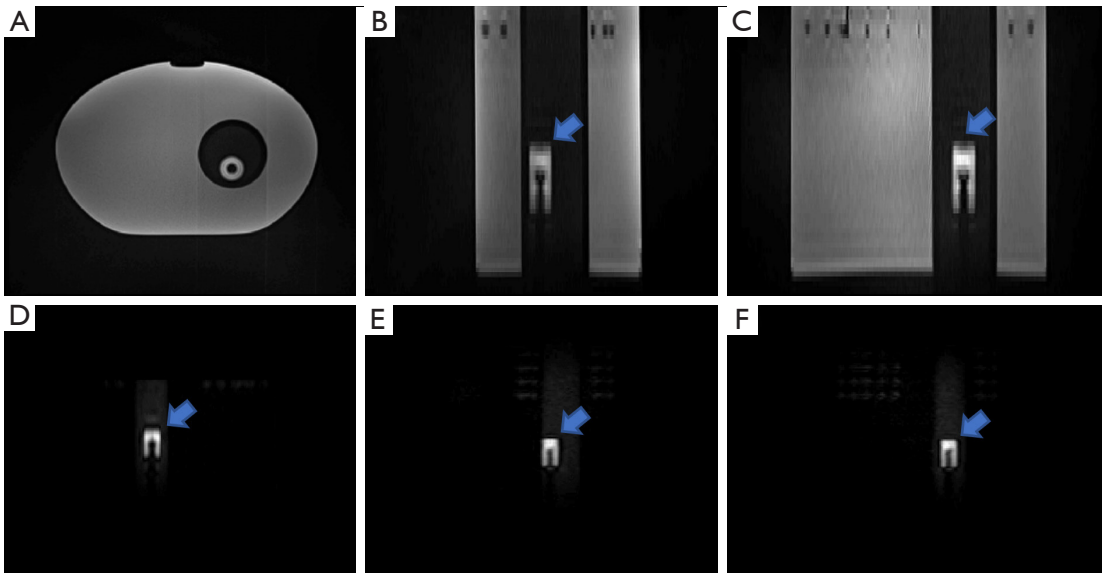

Figure 4 The CIRS phantom images with motion amplitude of 1.0 cm. (A-C) 3D T1W images in the axial, sagittal, and coronal views, respectively. (D-F) One frame of 4D-MRI images in the axial, sagittal, and coronal views, respectively. 3D, three-dimensional; MRI, magnetic resonance imaging; T1W, T1-weighted.

Table 1 Phantom motion measurement in coronal and sagittal views

Phantom motion amplitude (cm)	MMA (cm)			AMA (cm)		
	SI (coronal/sagittal)	AP (axial/sagittal)	ML (axial/sagittal)	SI (coronal/sagittal)	AP (axial/sagittal)	ML (axial/sagittal)
1.0	1.0/1.1	0.9/1.1	0.9/1.1	0.9/0.9	0.8/0.9	0.8/0.9
2.0	2.0/2.1	2.1/2.1	2.1/2.1	1.9/1.9	1.9/1.9	1.9/1.9
3.0	3.0/3.1	3.3/3.1	3.3/3.1	2.8/2.8	2.9/2.8	2.9/2.8
4.0	3.9/4.1	4.1/4.1	3.9/4.1	3.9/3.9	3.8/3.9	3.8/3.9

AMA, average motion amplitude; AP, anterior-posterior; ML, medium-lateral; MMA, maximum motion amplitude; SI, superior-inferior.

Table 1. The results showed that the measured motion agrees with the programmed motion with errors less than 3.0 mm. Examples of motion trajectories with different amplitudes in SI direction measured in sagittal view are shown in *Figure 5*. The measured motion trajectories agree well with the motion trajectories programmed for the phantom and the differences are generally less than 2.0 mm.

Patients study

Figure 6 shows an example of different MRI images of a liver cancer patient. *Figure 7* is a comparison of 2D Cine MRI and retrospectively sorted 4D-MRI based on amplitude in coronal view for a liver cancer patient. The image quality measurement results of the 4D-MRI in patients are shown in *Table 2*. No significant difference (P value >0.05) was found between 4D-MRI$_{CE}$/4D-MRI$_{NC}$ and T1W/T2W/2D Cine MRI for tumor SNR and CNR, while the liver SNR of 4D-MRI$_{CE}$ and 4D-MRI$_{NC}$ is significantly higher (P value <0.05) than T1W/T2W/2D Cine MRI. The mean MMA and AMA (± standard deviation, SD) measured for 4D-MRI$_{CE}$, 4D-MRI$_{NC}$, and Cine MRI for all patients are shown in *Table 3*. The mean absolute differences (MAD) of both maximum (MMA) and average (AMA) motion amplitudes between the two 4D-MRI sequences (4D-MRI$_{CE}$ and 4D-MRI$_{NC}$) and Cine MRI were small across all directions (SI, AP, ML), with no statistically significant differences observed between the sequences. For AMA, the P values were 0.096, 0.019, and 0.009 in the SI, AP, and ML directions respectively for

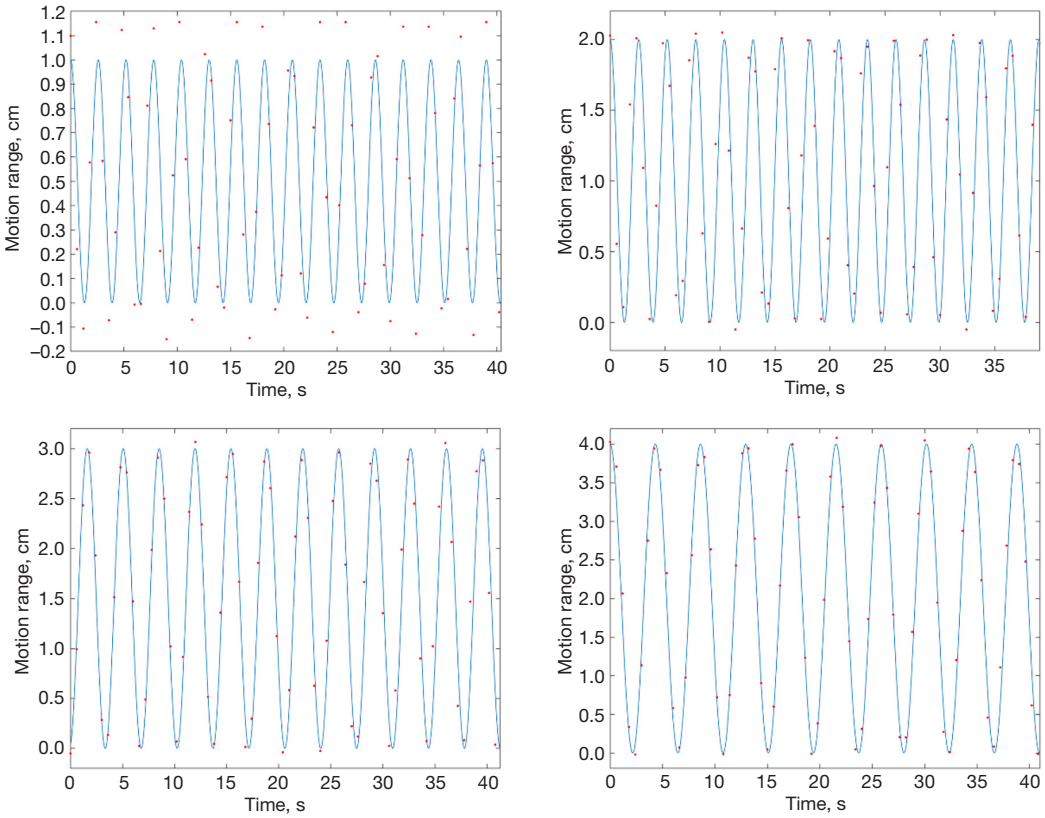

Figure 5 The measured motion trajectories in SI direction with amplitudes of 1.0, 2.0, 3.0, and 4.0 cm. The red dots are the measured position of the phantom motion bar, and the sinusoidal curves are the motion trajectories set by the CIRS phantom program. CIRS, Computerized Imaging Reference Systems, Inc.; SI, superior-inferior.

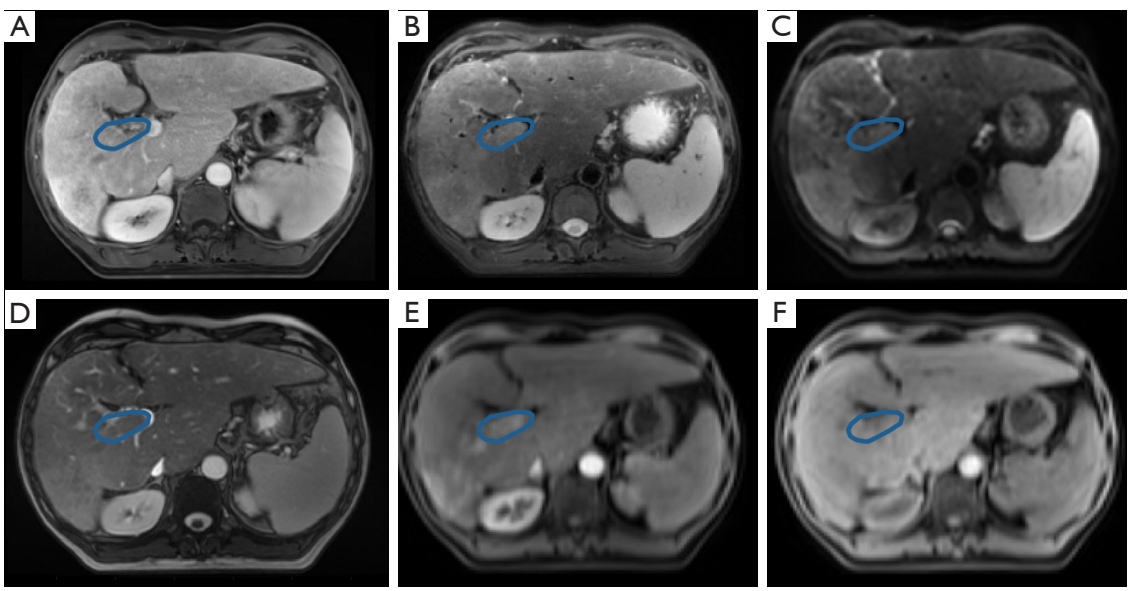

Figure 6 MRI images of an example patient. (A) T1W MRI. (B) T2W MRI. (C) DWI with b=800 s/mm^2. (D) Axial 2D Cine MRI. (E) 4D-MRI$_{CE}$. (F) 4D-MRI$_{NC}$. The blue outline indicates the position of the lesion. 4D-MRI, four-dimensional magnetic resonance imaging; 4D-MRI$_{CE}$, contrast-enhanced 4D-MRI; 4D-MRI$_{NC}$, non-contrast 4D-MRI; DWI, diffusion-weighted imaging; T1W, T1-weighted; T2W, T2-weighted.

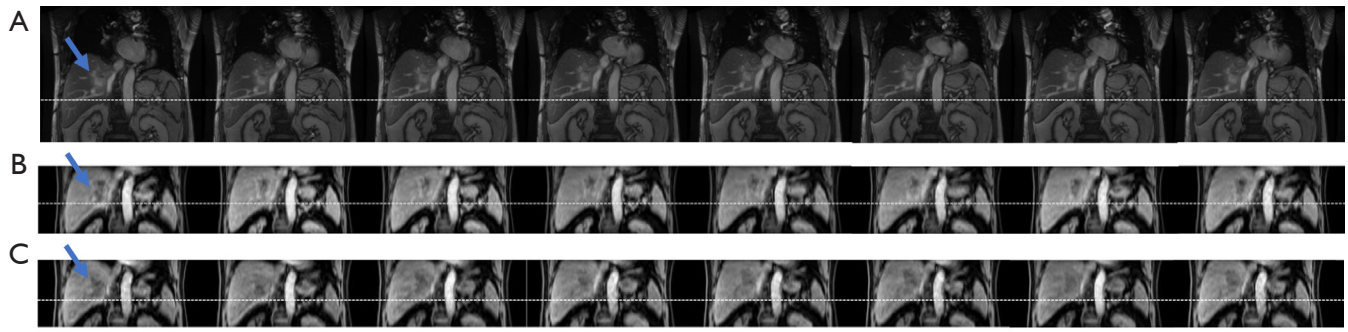

Figure 7 Coronal view of MRI images of an example patient. (A) 2D Cine MRI. (B) 4D-MRI$_{CE}$. (C) 4D-MRI$_{NC}$. The blue arrow indicates the position of the lesion, and the white dashed line is used to better visualize the motion. 2D, two-dimensional; 4D-MRI, four-dimensional magnetic resonance imaging; 4D-MRI$_{CE}$, contrast-enhanced 4D-MRI; 4D-MRI$_{NC}$, non-contrast 4D-MRI.

Table 2 Image quality measurement of 4D-MRI

Image quality index	4D-MRI$_{CE}$	4D-MRI$_{NC}$	T1W	T2W	Cine
SNR tumor	19.5±12.3**	21.8±8.2**	13.8±11.3	16.1±5.6	31.4±26.3
SNR liver	56.4±30.5	62.4±39.2	39.1±10.6	22.2±12.8	33.0±16.5
CNR	6.0±5.8**	5.2±4.3**	9.0±5.5	11.7±11.6	4.8±3.9

Data are presented as mean ± standard deviation. Statistical comparisons indicate results of a paired *t*-test comparing the SNR tumor and CNR between 4D-MRI and Cine for each patient in the category. **, P≤0.05. 4D-MRI, four-dimensional magnetic resonance imaging; 4D-MRI$_{CE}$, contrast-enhanced 4D-MRI; 4D-MRI$_{NC}$, non-contrast 4D-MRI; CNR, contrast-to-noise rations; SNR, signal-to-noise ratio; T1W, T1-weighted; T2W, T2-weighted.

Table 3 Patients motion measurement in three directions

Image modalities	MMA (cm)			AMA (cm)		
	SI	AP	ML	SI	AP	ML
4D-MRI$_{CE}$	1.31±0.48*	0.31±0.18**	0.19±0.13***	1.07±0.47*	0.28±0.11**	0.17±0.13***
4D-MRI$_{NC}$	1.32±0.52**	0.33±0.16***	0.19±0.12**	1.00±0.49**	0.30±0.07***	0.17±0.13**
Cine	1.25±0.39	0.26±0.19	0.14±0.08	1.06±0.40	0.23±0.20	0.12±0.05

Statistical comparisons indicate results of a paired *t*-test comparing the mean motion amplitude for each patient in the category. *, P≤0.1; **, P≤0.05; ***, P≤0.01. 4D-MRI, four-dimensional magnetic resonance imaging; 4D-MRI$_{CE}$, contrast-enhanced 4D-MRI; 4D-MRI$_{NC}$, non-contrast 4D-MRI; AMA, average motion amplitude; AP, anterior-posterior; ML, medium-lateral; MMA, maximum motion amplitude; SI, superior-inferior.

4D-MRI$_{CE}$, and 0.049, 0.008, and 0.016 for 4D-MRI$_{NC}$. For MMA, the P values were 0.054, 0.022, and 0.086 for 4D-MRI$_{CE}$, and 0.041, 0.007, and 0.016 for 4D-MRI$_{NC}$. A slight inconsistency in motion along the SI direction was noted in the 4D-MRI$_{CE}$ sequence, likely attributable to motion artifacts.

Discussion

Recent studies of SBRT have demonstrated improved treatment outcomes for abdominal cancer patients. However, the application of radiotherapy in abdominal cancers has been historically limited by the tumor motion introduced by respiration. Therefore, various

methods have been proposed to measure tumor motion for motion management in radiotherapy, including 4D-CT, Cine MRI, 4D-MRI, etc. Among these methods, 4D-MRI has gained increasing attention recently due to its excellent soft-tissue contrast, ability of providing 3D motion information, and has no radiation hazard. Nevertheless, most current 4D-MRI techniques require sophisticated software or hardware which have greatly hindered its clinical applications. Therefore, in this study, we evaluated a commercially available 4D-MRI method for abdominal tumor motion management. A previous study has demonstrated the feasibility of using controlled aliasing in parallel imaging results in higher acceleration (CAIPIRINHA)-VIBE sequence for fast volumetric 4D-MRI acquisition with 0.615 s/measurement and has demonstrated better volumetric consistency compared with a 2D-HASTE 4D-MRI method (16). However, they only included nine volunteers in the study and did not evaluate their technique against clinical standard or physical phantoms. The TWIST-VIBE sequence was originally designed for contrast enhanced imaging. It uses the CAIPIRINHA and keyhole techniques to accelerate the acquisition speed and is able to acquire multiple 3D volumes within seconds, which provides the possibility for 4D-MRI application in radiotherapy. Compared to other 4D-MRI methods using 3D acquisition, it does not require sophisticated hardware or software and has a faster scanning time (50 s *vs.* several minutes) (17). In this study, we have conducted a more comprehensive evaluation of the commercially available 4D-MRI based on TWIST-VIBE sequence in four volunteers and 34 patients. The commercially available 4D-MRI technique was compared with the Cine MRI which is a clinical standard method for tumor motion measurement and validated using a physical motion phantom. The evaluation results of this study could provide helpful information for clinical adoption of this commercially available 4D-MRI technique.

The MR compatible physical phantom used for validation in this study was set to move sinusoidally with different motion amplitudes in SI direction. For the motion in AP and ML directions, it was achieved by rotating of the motion rod with different degrees. In *Figure 4*, it can be seen that the motion of the phantom will introduce blurring artifacts in the clinical 3D T1W image while the boundary can be clearly identified in the 4D-MRI images. This indicates that the 4D-MRI may provide a more accurate and conformal tumor delineation in radiotherapy which in turn may improve the dose conformity to the target and spare more normal tissues around the target. The measured AMA and MMA in three directions generally agree well with the programmed motion of the phantom with maximum error of 2.0 mm as shown in *Table 1*, indicating a satisfactory motion measurement accuracy of this 4D-MRI technique. The motion measurement data points in *Figure 5* were retrospectively fitted to a sinusoidal curve with programmed amplitude and have also demonstrated a good agreement with an error around 2.0 mm. The results of phantom experiments demonstrated satisfactory motion measurement accuracy of this 4D-MRI technique, indicating a good potential for the clinical adoption of this technique.

The 4D-MRI was acquired both before and immediately after the contrast agent injection to evaluate potential influences of contrast-agent on the image quality of 4D-MRI. It can be seen from the quantitative evaluation results in *Table 2* that the tumor SNR, liver SNR, and tumor CNR are similar for both 4D-MRI_{CE} and 4D-MRI_{NC} with no significant differences. However, we have observed that for 4D-MRI_{CE}, the liver signal generally becomes higher with time after contrast agent injection, which makes the boundary of liver become clearer. Since the 4D-MRI acquisition time is relatively short and is unlikely to interfere with the clinical practice, acquiring 4D-MRI after contrast-injection may improve the motion measurement accuracy. Nevertheless, future studies are still warranted to verify this observation. In addition, motion artifacts were also observed in certain frames of 4D-MRI_{CE} and 4D-MRI_{NC} for several patients which may be caused by the breathing irregularity during acquisition, and this may also be the reason why relatively large variation of SNR measurement in 4D-MRI_{CE} and 4D-MRI_{NC} are observed.

For motion measurement in the liver cancer patients, although the 4D-MRI and Cine MRI were acquired at different time points, the differences of MMA and AMA between 4D-MRI and Cine MRI are relatively small with no significant differences. However, it is worth noticing that the Cine MRI was acquired with a frame rate of 0.26 s/frame, which is faster than the 4D-MRI frame rate of 0.69 s/measurement, and this may render the Cine MRI more sensitive to the measurement of motion trajectory. The relatively slow frame rate of 4D-MRI may introduce some motion artifacts and blur the image if irregular breathing happens. However, with a scanning time of 50 seconds, we can acquire more than 70 frames and it could cover most of the major breathing status and the motion measurement results are satisfactory. Therefore, with a clinically acceptable scanning time, we believe

this technique can provide useful motion information for tumour or OAR in the field of radiotherapy. In addition, the voxel size of the 4D-MRI is isotopically 2.7 mm^3 which may lose some anatomical details as can be seen in *Figure 6* and is not optimal for radiotherapy applications. Therefore, future studies are warranted to further improve both the temporal and spatial resolutions of 4D-MRI to make the motion measurement more precise. One possible solution is to use MRI super resolution techniques to enhance image quality. There are several super resolution techniques available including the one we proposed (18-22). However, their efficacy on the 4D-MRI needs to be evaluated in the future study. Another limitation of the fast volumetric 4D-MRI technique is the compromised image contrast which may make it challenging to identify the tumor accurately. However, studies have reported that the 3D imaging techniques can provide satisfactory registration accuracy (23-25). Therefore, one possible solution is to extract the deformation vector fields from the 4D-MRI and apply it on the high-quality static 3D MRI sets (26). Nevertheless, the clinical efficacy of this method still needs to be verified.

There are several limitations in this study, which also suggest promising directions for future work:

- First, the evaluated fast volumetric 4D-MRI technique was implemented only on a single machine from one vendor (3.0 T Skyra, Siemens). Its feasibility and performance on scanners from other vendors or field strengths remain untested, which may limit the generalizability of the proposed approach. Future investigations are necessary to validate the technique across diverse platforms and hardware configurations.
- Second, this study only evaluated a single spatial-temporal resolution setting (0.69 s/measurement with isotropic 2.7 mm3 voxels), selected as a practical balance between image quality and temporal resolution. However, in MR-guided radiotherapy, clinical demands vary greatly—some scenarios may benefit from higher temporal resolution with coarser spatial detail, while others require submillimeter precision for accurate target delineation (27). Future work will systematically explore a broader matrix of acquisition strategies, pairing in-plane resolutions (e.g., 1.0, 1.5, and 2.0 mm) with temporal resolutions spanning 2–20 Hz. Advanced k-space sampling techniques (e.g., golden-angle radial, variable-density spiral) and cutting-edge reconstruction algorithms (e.g., compressed sensing, low-rank models, and deep-learning-based unrolled networks) will also be incorporated to optimize spatiotemporal trade-offs for clinical scenarios such as gating, dose accumulation, and adaptive replanning.
- Third, the current patient scans were acquired under immobilization without concurrent respiratory monitoring, which prevented correlation with real-time breathing waveforms or assessment of irregular respiratory patterns on image quality. To address this, we are conducting phantom-based experiments using programmable respiratory phantoms capable of replicating complex, patient-derived breathing profiles (e.g., apnea, deep breaths, coughing), along with synchronized optical motion tracking (28). These will allow quantitative comparisons of motion accuracy, image fidelity, and gating trigger performance under varied respiratory conditions. Furthermore, future *in vivo* studies with integrated respiratory sensors (e.g., bellows, navigator echoes) will enable correlation between external motion surrogates and image-derived trajectories, paving the way for adaptive reconstruction schemes and robust outlier rejection mechanisms.
- Lastly, although this study demonstrates technical improvements in motion imaging, the clinical impact on radiotherapy planning remains to be quantified. Future studies will integrate reconstructed 4D-MRI into treatment planning systems to evaluate its dosimetric benefits, such as margin reduction and sparing of healthy tissues. Comparative analysis between conventional planning workflows and those using motion-informed contours derived from our method will be conducted to assess improvements in targeting accuracy and treatment adaptation.

Conclusions

We evaluated the feasibility of a commercially available TWIST-VIBE 4D-MRI sequence for motion management in liver cancer radiotherapy. Preliminary assessments of image quality and motion measurement accuracy demonstrated satisfactory performance, supporting its potential for clinical application.

Acknowledgments

A preliminary idea of this work has been collected as an

abstract and presented at the ISMRM conference (https://cds.ismrm.org/protected/21MProceedings/PDFfiles/4017.html).

Footnote

Reporting Checklist: The authors have completed the STARD reporting checklist. Available at https://qims.amegroups.com/article/view/10.21037/qims-2025-1039/rc

Data Sharing Statement: Available at https://qims.amegroups.com/article/view/10.21037/qims-2025-1039/dss

Funding: TThis study was supported by: (I) The National Natural Science Foundation of China Young Scientist Fund from China (NSFC-YSF 82202941); (II) The Innovation and Technology Support Program from the Hong Kong Special Administrative Region (HKSAR), China (ITS/049/22FP); (III) The General Research Fund from HKSAR, China (GRF 15104822, GRF 15102219); (IV) The Health and Medical Research Fund from HKSAR, China (HMRF 10211606 and HMRF 06173276); (V) The Research Project Grant of the National Institutes of Health from the United States (NIH R01 CA226899); (VI) Ministry of Education Exchange Program for Teachers and Students of Higher Education Institutions in the Chinese Mainland/Hong Kong/Macao (7111400072).

Conflicts of Interest: All authors have completed the ICMJE uniform disclosure form (available at https://qims.amegroups.com/article/view/10.21037/qims-2025-1039/coif). The authors have no conflicts of interest to declare.

Ethical Statement: The authors are accountable for all aspects of the work in ensuring that questions related to the accuracy or integrity of any part of the work are appropriately investigated and resolved. The study was approved by ethics board of Peking University Cancer Hospital & Institute (No. 2021YJZ05), and informed consent was taken from all the patients. This study was conducted in accordance with the Declaration of Helsinki and its subsequent amendments.

References

1. Ferlay J, Ervik M, Lam F, Colombet M, Mery L, Piñeros M, et al. Global Cancer Observatory: Cancer Today. International Agency for Research on Cancer; 2020. Available online: https://gco.iarc.fr/today
2. Murray LJ, Dawson LA. Advances in Stereotactic Body Radiation Therapy for Hepatocellular Carcinoma. Semin Radiat Oncol 2017;27:247-55.
3. Wild AT, Yamada Y. Treatment Options in Oligometastatic Disease: Stereotactic Body Radiation Therapy - Focus on Colorectal Cancer. Visc Med 2017;33:54-61.
4. Fast M, van de Schoot A, van de Lindt T, Carbaat C, van der Heide U, Sonke JJ. Tumor Trailing for Liver SBRT on the MR-Linac. Int J Radiat Oncol Biol Phys 2019;103:468-78.
5. Gani C, Boeke S, McNair H, Ehlers J, Nachbar M, Mönnich D, Stolte A, Boldt J, Marks C, Winter J, Künzel LA, Gatidis S, Bitzer M, Thorwarth D, Zips D. Marker-less online MR-guided stereotactic body radiotherapy of liver metastases at a 1.5 T MR-Linac - Feasibility, workflow data and patient acceptance. Clin Transl Radiat Oncol 2021;26:55-61.
6. Hall WA, Straza MW, Chen X, Mickevicius N, Erickson B, Schultz C, Awan M, Ahunbay E, Li XA, Paulson ES. Initial clinical experience of Stereotactic Body Radiation Therapy (SBRT) for liver metastases, primary liver malignancy, and pancreatic cancer with 4D-MRI based online adaptation and real-time MRI monitoring using a 1.5 Tesla MR-Linac. PLoS One 2020;15:e0236570.
7. Méndez Romero A, Wunderink W, Hussain SM, De Pooter JA, Heijmen BJ, Nowak PC, Nuyttens JJ, Brandwijk RP, Verhoef C, Ijzermans JN, Levendag PC. Stereotactic body radiation therapy for primary and metastatic liver tumors: A single institution phase i-ii study. Acta Oncol 2006;45:831-7.
8. Chang DT, Schellenberg D, Shen J, Kim J, Goodman KA, Fisher GA, Ford JM, Desser T, Quon A, Koong AC. Stereotactic radiotherapy for unresectable adenocarcinoma of the pancreas. Cancer 2009;115:665-72.
9. Rwigema JC, Parikh SD, Heron DE, Howell M, Zeh H, Moser AJ, Bahary N, Quinn A, Burton SA. Stereotactic body radiotherapy in the treatment of advanced adenocarcinoma of the pancreas. Am J Clin Oncol

2011;34:63-9.
10. Crane CH, Koay EJ. Solutions that enable ablative radiotherapy for large liver tumors: Fractionated dose painting, simultaneous integrated protection, motion management, and computed tomography image guidance. Cancer 2016;122:1974-86.
11. Low D. 4D imaging and 4D radiation therapy: a New Era of therapy design and delivery. Front Radiat Ther Oncol 2011;43:99-117.
12. Akino Y, Oh RJ, Masai N, Shiomi H, Inoue T. Evaluation of potential internal target volume of liver tumors using cine-MRI. Med Phys 2014;41:111704.
13. Nonaka H, Onishi H, Watanabe M, Nam VH. Assessment of abdominal organ motion using cine magnetic resonance imaging in different gastric motilities: a comparison between fasting and postprandial states. J Radiat Res 2019;60:837-43.
14. Cai J, Chang Z, Wang Z, Paul Segars W, Yin FF. Four-dimensional magnetic resonance imaging (4D-MRI) using image-based respiratory surrogate: a feasibility study. Med Phys 2011;38:6384-94.
15. Du D, Caruthers SD, Glide-Hurst C, Low DA, Li HH, Mutic S, Hu Y. High-quality t2-weighted 4-dimensional magnetic resonance imaging for radiation therapy applications. Int J Radiat Oncol Biol Phys 2015;92:430-7.
16. Yuan J, Wong OL, Zhou Y, Chueng KY, Yu SK. A fast volumetric 4D-MRI with sub-second frame rate for abdominal motion monitoring and characterization in MRI-guided radiotherapy. Quant Imaging Med Surg 2019;9:1303-14.
17. Deng Z, Pang J, Yang W, Yue Y, Sharif B, Tuli R, Li D, Fraass B, Fan Z. Four-dimensional MRI using three-dimensional radial sampling with respiratory self-gating to characterize temporal phase-resolved respiratory motion in the abdomen. Magn Reson Med 2016;75:1574-85.
18. Huang B, Xiao H, Liu W, Zhang Y, Wu H, Wang W, Yang Y, Yang Y, Miller GW, Li T, Cai J. MRI super-resolution via realistic downsampling with adversarial learning. Phys Med Biol 2021;66:10.1088/1361-6560/ac232e.
19. Manjón JV, Coupé P, Buades A, Fonov V, Louis Collins D, Robles M. Non-local MRI upsampling. Med Image Anal 2010;14:784-92.
20. Luo J, Mou Z, Qin B, Li W, Yang F, Robini M, Zhu Y. Fast single image super-resolution using estimated low-frequency k-space data in MRI. Magn Reson Imaging 2017;40:1-11.
21. Shi J, Li Z, Ying S, Wang C, Liu Q, Zhang Q, Yan P. MR Image Super-Resolution via Wide Residual Networks With Fixed Skip Connection. IEEE J Biomed Health Inform 2019;23:1129-40.
22. Lim B, Son S, Kim H, Nah S, Mu Lee K. Enhanced deep residual networks for single image super-resolution. 2017 IEEE Conference on Computer Vision and Pattern Recognition Workshops (CVPRW); 21-26 July 2017; Honolulu, HI, USA. IEEE; 2017.
23. Stemkens B, Tijssen RH, de Senneville BD, Heerkens HD, van Vulpen M, Lagendijk JJ, van den Berg CA. Optimizing 4-dimensional magnetic resonance imaging data sampling for respiratory motion analysis of pancreatic tumors. Int J Radiat Oncol Biol Phys 2015;91:571-8.
24. Glitzner M, de Senneville BD, Lagendijk JJ, Raaymakers BW, Crijns SP. On-line 3D motion estimation using low resolution MRI. Phys Med Biol 2015;60:N301-10.
25. Roujol S, Ries M, Moonen C, de Senneville BD. Automatic nonrigid calibration of image registration for real time MR-guided HIFU ablations of mobile organs. IEEE Trans Med Imaging 2011;30:1737-45.
26. Xiao H, Ni R, Zhi S, Li W, Liu C, Ren G, Teng X, Liu W, Wang W, Zhang Y, Wu H, Lee HV, Cheung LA, Chang HC, Li T, Cai J. A dual-supervised deformation estimation model (DDEM) for constructing ultra-quality 4D-MRI based on a commercial low-quality 4D-MRI for liver cancer radiation therapy. Med Phys 2022;49:3159-70.
27. Feng L, Grimm R, Block KT, Chandarana H, Kim S, Xu J, Axel L, Sodickson DK, Otazo R. Golden-angle radial sparse parallel MRI: combination of compressed sensing, parallel imaging, and golden-angle radial sampling for fast and flexible dynamic volumetric MRI. Magnetic Resonance in Medicine 2013;72:707-17.
28. Dunn L, Kron T, Johnston PN, McDermott LN, Taylor ML, Callahan J, Franich RD. A programmable motion phantom for quality assurance of motion management in radiotherapy. Australas Phys Eng Sci Med 2012;35:93-100.

Cite this article as: Wang P, Liu W, Xiao H, Liu C, Li W, Ren G, Zhang Y, Wu H, Wang W, Cai J, Li T. Evaluation of a fast-volumetric four-dimensional magnetic resonance imaging technique for abdominal radiotherapy tumor motion management. Quant Imaging Med Surg 2025;15(10):10050-10061. doi: 10.21037/qims-2025-1039